Mon. Not. R. Astron. Soc. **298,** 525–536 (1998)

Stellar evolution models for $Z = 0.0001$ to 0.03

Onno R. Pols,[1,2⋆] Klaus-Peter Schröder,[3,2⋆] Jarrod R. Hurley,[2⋆] Christopher A. Tout[2⋆] and Peter P. Eggleton[2⋆]

[1] *Instituto de Astrofísica de Canarias, c/ Via Láctea s/n, E-38200 La Laguna, Tenerife, Spain*
[2] *Institute of Astronomy, Madingley Road, Cambridge CB3 0HA*
[3] *Institut für Astronomie und Astrophysik, Hardenbergstrasse 36, D-10623 Berlin, Germany*

Accepted 1998 March 13. Received 1998 March 13; in original form 1998 January 15

ABSTRACT

We have calculated a grid of empirically well tested evolutionary tracks with masses M between 0.5 and 50 $M_\odot$, spaced by approximately 0.1 in $\log M$, and with metallicities $Z = 0.0001$, 0.0003, 0.001, 0.004, 0.01, 0.02 and 0.03. We use a robust and fast evolution code with a self-adaptive non-Lagrangian mesh, which employs the mixing-length theory but treats convective mixing as a diffusion process, solving simultaneously for the structure and the chemical composition. The hydrogen and helium abundances are chosen as functions of the metallicity: $X = 0.76 - 3.0Z$ and $Y = 0.24 + 2.0Z$.

Two sets of models were computed, one without and one with a certain amount of enhanced mixing or 'overshooting'. This amount has been empirically chosen by means of various sensitive tests for overshooting: (1) the luminosity of core helium burning (blue loop) giants of well-known mass, (2) the width of the main sequence as defined by double-lined eclipsing binaries with well-measured masses and radii, and (3) the shape and implied stellar distribution of isochrones of various open clusters. The first two tests have been the subject of previous papers, the third test is discussed in this paper. On the basis of these tests, we recommend the use of the overshooting models for masses above about 1.5 $M_\odot$.

We describe here the characteristics of the models, the procedure for constructing isochrones for arbitrary age and metallicity from the models, and the performance of these isochrones for several intermediate-age and old open clusters. All original models are available in electronic form and we describe the means by which they may be obtained.

Key words: convection – stars: evolution – Hertzsprung–Russell (HR) diagram – stars: Population II – open clusters and associations: general – galaxies: stellar content.

1 INTRODUCTION

The development of stellar evolution codes started more than four decades ago and from today's astrophysics textbooks it appears to be a well-understood problem. Indeed, a good understanding has been achieved – at least qualitatively – of the many physical processes involved in the various evolutionary stages. In fact, stellar evolution is related to many fields of modern physics, nuclear physics, particle physics, atomic and molecular physics, thermodynamics, hydrodynamics, the physics of radiation and its interaction with matter, and radiative transfer. As an introduction to the problems of stellar evolution in general, and to some of its vast literature, we only cite Kippenhahn & Weigert (1991), Chiosi (1992) and VandenBerg (1991).

⋆E-mail: onno@ll.iac.es (ORP); schroder@weizen.physik.tu-berlin.de (K-PS); jhurley@ast.cam.ac.uk (JRH); cat@ast.cam.ac.uk (CAT); ppe@ast.cam.ac.uk (PPE)

There is a definite need for quantitatively reliable results of stellar evolution in other fields of astrophysics. In galactic astrophysics, stars are more than just one constituent of a galaxy. The stellar population interacts with the interstellar matter in various ways. The combined radiation field is an important quantity, as is the effect that stellar winds and supernovae have on the chemical evolution of any galaxy. Furthermore, in cosmology the age of globular clusters is of utmost importance as one of the most stringent constraints to, for example, the value of the Hubble constant and the mean density.

Nevertheless, the unsolved 'solar neutrino problem' is perhaps the most prominent reminder that there is still some way to go before we have accomplished a really good *quantitative* understanding of stellar evolution, even though large efforts have recently been put into improving the quantitative performance of modern evolutionary codes. Much work has been devoted to the atomic and molecular opacities, as required for a wide range of frequencies and temperatures (e.g. OPAL, Rogers & Iglesias 1992 and Iglesias & Rogers 1996; Seaton et al. 1994; Alexander & Ferguson 1994a,b),

as well as the various nuclear reaction rates (Caughlan & Fowler 1988) and the neutrino losses (Itoh et al. 1989, 1992, 1996). Armed with these new achievements, results from improved evolutionary codes have been presented in the recent past (see for example Schaller et al. 1992, Bressan et al. 1993 and Claret 1995).

While this progress has indeed significantly improved the match between theory and observation (see for example the study of cluster isochrones by Meynet, Mermilliod & Maeder 1993), especially for the domains of cool and very evolved stars, virtually all current codes still have the same Achilles heel. It is the physically crude description of convection, mostly based on the mixing-length theory (Böhm-Vitense 1958; Baker & Temesvary 1966). Mixing-length theory persists partly because of its simplicity and efficiency – particularly in its dependence on only local stellar structure, a requirement of the solution techniques used in stellar evolution codes – and partly because realistic simulations of convection still lie beyond our computational abilities (Singh, Roxburgh & Kwing 1994). We note here that an absolute theory of convection would remove the essentially free parameter $\alpha = l/H_{\rm p}$, the ratio of typical mixing length to the local pressure scaleheight, that allows us to precisely fit the radius of the Sun. A parameter-free convection model was developed by Canuto & Mazzitelli (1991, 1992).

Indeed, convection is by far the most efficient means of energy transfer in a star, except very close to the photosphere. Stars with effective temperatures $T_{\rm eff} \leq 6500$ K develop deep outer convection zones, and the model parameters $T_{\rm eff}$ and radius depend strongly on the representation of this convection. By contrast, stars which are more massive than the Sun have convective cores. In these, convective mixing is a vital factor during the core hydrogen burning phase, with importance for the life-times of the core hydrogen (and later helium) burning phases and the luminosities of evolved models.

A second adjustable parameter, the distance $l_{\rm ov}$ of 'overshooting' of convective elements into non-convective layers, stems from another simplification of mixing-length theory, the possibility of mixing processes *beyond* the expected boundary of convective instability. Mixing could in fact reach into regions which are supposed to be stable, according to the well-known Schwarzschild criterion (Shaviv & Salpeter 1973). From the naive approach of mixing-length theory the intuitive name 'overshooting' is used for such a process, but we must keep in mind that *any* enhanced mixing can be described in this way. In any case, enhanced mixing enlarges the reservoir of hydrogen within reach of the hydrogen-burning core source. The resultant effect is a prolonged main-sequence lifetime, an enhanced helium core thereafter, and a more luminous but shorter-lived core helium burning giant – found in its blue loop. A brief summary of the effects related to core overshooting in intermediate-mass and massive stars has been given by Schröder, Pols & Eggleton (1997, hereafter Paper II).

For these reasons, empirical tests are needed to constrain the crucial choice of the two adjustable parameters which are inevitably introduced by the mixing-length theory, α and $l_{\rm ov}$. Our idea of presenting a new grid of evolutionary tracks is therefore not only founded on the different philosophy of our code, which – although based on the mixing length approach – accounts for enhanced mixing not by a prescribed overshooting length, but by a modification of the stability criterion itself (see Section 2). Rather, we have imposed various empirical tests on the quantification of the parameters of the code (see Paper II and Pols et al. 1997, hereinafter Paper III), because we wish to provide stellar evolution tracks which are an accurate tool for applying quantitative applications to problems of global character, such as the evolution of stellar activity (Hünsch & Schröder 1996), population synthesis in *N*-body calculations (Tout et al. 1997), and galactic astrophysics.

A more sophisticated convection theory, or a large-scale approach to convection by numerical simulation, may finally yield the required amount of enhanced mixing in a self-consistent way, without any adjustable parameter. Until such models are available, however, the empirically well-calibrated evolutionary tracks presented here are a good representation of real stars, despite the fact that they have been computed with an economical code.

There are two alternative approaches to the problem of using the output of a series of stellar-evolutionary runs as data for projects that require them, such as population synthesis. One approach is to construct tables (necessarily rather large especially if a range of metallicities and/or overshoot parameters is to be incorporated) and interpolate within these tables. This is the approach of this paper (Section 5). The other is to approximate the data by a number of interpolation formulae. Both procedures have advantages and disadvantages (Eggleton 1996), and so we have worked on both approaches simultaneously. We are constructing interpolated evolution formulae as functions of age, mass and metallicity, thus expanding the work of Eggleton, Fitchett & Tout (1989) along the lines of Tout et al. (1996). This is still in progress (Hurley et al., in preparation). It is more difficult, in practice, to find analytic approximations of a conveniently simple nature for the highly non-uniform movement of a star in the HR diagram than it is to interpolate in tables, but the resulting code can be very much more compact and adaptable to the requirements of, for example, an *N*-body code (Aarseth 1996) or variable mass loss. This is reinforced in the circumstance in which one wishes to include binary star interactions, such as (for example) Roche lobe overflow, common-envelope evolution, and magnetic braking with tidal friction (Tout et al. 1997).

2 THE EVOLUTION CODE

We use a robust and fast evolution code, which is based on the original evolution program of Eggleton (1971, 1972, 1973). The essential features of that code, in which it deviates from other codes and which have survived unaltered in the present version, are: (a) the use of a self-adaptive, non-Lagrangian mesh, (b) the treatment of both convective and semiconvective mixing as a diffusion process, and (c) the simultaneous and implicit solution of both the stellar structure equations and the diffusion equations for the chemical composition. These characteristics are advantageous especially for the evolved stages with one or two thin shell sources, avoiding the need for a redistribution of mesh points. In the present version the non-Lagrangian mesh-spacing is a function of the local pressure $P(r)$, temperature $T(r)$, Lagrangian mass $m(r)$ and radius r. A stellar model is well represented by only 200 mesh points at any stage of its evolution up to central carbon burning. This saves computation time and makes the code easy to use.

The most important recent update of the code, described by Pols et al. (1995, hereinafter Paper I), was the improvement of the original equation of state (Eggleton, Faulkner & Flannery 1973) by the inclusion of pressure ionization and Coulomb interactions, and the incorporation of recent opacity tables (derived from Rogers & Iglesias 1992 and Alexander & Ferguson 1994a,b), nuclear reaction rates (from Caughlan & Fowler 1988 and Caughlan et al. 1985) and neutrino loss rates (Itoh et al. 1989, 1992). Other changes and improvements to the code over the last 20 yr have not been recorded systematically, but some of them have been summarized by Han,

Podsiadlowski & Eggleton (1994). It is worth mentioning here that mass loss (e.g. owing to stellar winds) can be almost trivially incorporated into the boundary conditions; however, we did not make use of this option for the calculations presented here (see Section 3 for a discussion).

Standard mixing-length theory is used by our code to describe the heat transport, therefore the structure of the outer layers of our stellar models depends on the choice of α. A good fit to the Sun by a realistic solar model yields $\alpha = 2.0$ as the most appropriate choice (see below). So far, the philosophy of our code is similar to most other contemporary evolutionary codes. However, our code treats convective mixing and semiconvection as diffusion processes with a diffusion rate adopted as a function of $\nabla_{\rm rad} - \nabla_{\rm ad}$. Since the mixing processes are vital to the evolution of the core, in particular to the luminosities and lifetimes associated with hydrogen and helium core burning, this point deserves special attention.

The other problem related to mixing, which is of greatest importance for all stellar models with convective cores (i.e. all models with masses M larger than about $1.1\,{\rm M}_\odot$), is the extent of mixing. Observational evidence has been accumulated over the past two decades which suggests that the assumption that mixing is confined exclusively to regions that are convectively unstable according to the Schwarzschild criterion is an inadequate simplification. Instead, enhanced mixing, i.e. mixing beyond the standard convective boundary, is needed to arrive at longer core hydrogen burning lifetimes by giving the core access to a larger reservoir of unprocessed plasma. For this effect the expression 'overshooting' has been adopted from the idea of convective cells pushing into the stable regions just beyond the convective boundary. We have adopted this name, but other processes of enhanced mixing, such as meridional circulation owing to strong rotation (e.g. Fliegner & Langer 1995, Talon et al. 1997) may also be involved. Our simple representation of overshooting does not distinguish between the various contributions to enhanced mixing but describes a combination of all such effects.

Unlike other approaches (e.g. Schaller et al. 1992, Bressan et al. 1993, Claret 1995), we do not parametrize the overshooting length $l_{\rm ov}$ in units of the pressure scaleheight $H_{\rm P}$ (which we call the '$H_{\rm P}$ prescription'). Instead, we base our treatment on the stability criterion itself, the '∇ prescription', by incorporating the condition that mixing occurs in a region with $\nabla_{\rm rad} > \nabla_{\rm ad} - \delta$. We define δ as the product of a free parameter $\delta_{\rm ov}$, our overshooting constant, and a conveniently chosen factor which depends only on the ratio ζ of radiation pressure to gas pressure: $\delta = \delta_{\rm ov}/(2.5 + 20\zeta + 16\zeta^2)$. The object of this ζ-dependence is to ensure that in massive stars, where ζ is relatively large and where both $\nabla_{\rm rad}$ and $\nabla_{\rm ad}$ are quite close to 0.25, the overshooting does not extend over the entire envelope. The ζ-dependent factor ensures, roughly, that mixing extends over a certain fraction of the pressure scaleheight rather than the entropy scaleheight, the latter being quite large if $\nabla_{\rm rad} \sim \nabla_{\rm ad}$. Our physical assumption is roughly that mixing occurs in regions which would be classically stable, provided that they are stable only by a small margin, δ. However, the temperature structure in this extended mixing region is still assumed to be radiative, not adiabatic.

Our intention was to avoid two unsatisfactory consequences of the $H_{\rm P}$ prescription: (a) since $H_{\rm P} \rightarrow \infty$ at the centre, a triflingly small core would generate an enormous additional mixing region; and (b) once the classical convective core shrinks to zero, the overshoot region abruptly shrinks to zero also. The ∇ prescription on the other hand gives a smooth decrease in the size of the overshoot region as $\nabla_{\rm r} - \nabla_{\rm a}$ at the centre decreases towards zero (Fig. 1). It is seen that, as the classical convective core disappears at $M = 1.17\,{\rm M}_\odot$, the ratio $l_{\rm ov}/H_{\rm P}$ also goes to zero as expected. However, for smaller masses a small central region remains which has $-\delta < \nabla_{\rm rad} - \nabla_{\rm ad} < 0$ and is thus homogeneously mixed (although not convective). Hence there is no physical discontinuity at the transition mass. Since the mixed region is small (much less than 10 per cent of the total mass) and we assume radiative transport in regions that are stable according to Schwarzschild, the structure of models with $M \lesssim 1\,{\rm M}_\odot$ is very similar to that of standard models, and the differences in luminosity, radius or lifetime are negligible. For $M > 1.17\,{\rm M}_\odot$, the ∇ prescription with $\delta_{\rm ov} = 0.12$ leads to a ratio $l_{\rm ov}/H_{\rm P}$ that varies between 0.22 and 0.4 at the low-mass and high-mass ends, respectively.

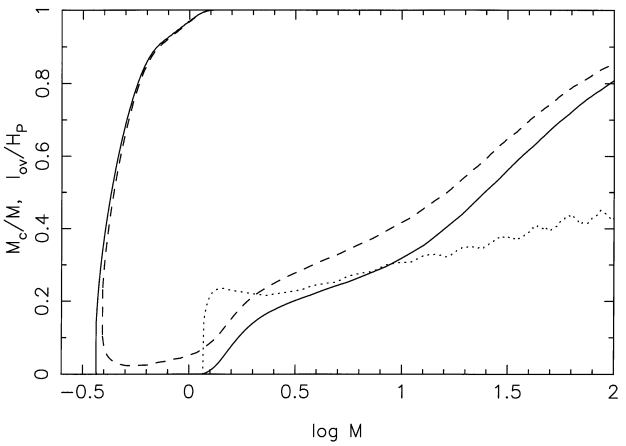

Figure 1. The effects of the '∇ prescription' with $\delta_{\rm ov} = 0.12$ on ZAMS models with $Z = 0.02$. As a function of stellar mass we show the mass fraction of the classical (Schwarzschild) convective core and envelope boundaries (solid line), the mass fraction of the overshoot regions (dashed line), and the core overshoot length $l_{\rm ov}$ divided by $H_{\rm P}$ at the Schwarzschild boundary (dotted line). For $M = 1.17\,{\rm M}_\odot$, the classical convective core disappears and the ratio $l_{\rm ov}/H_{\rm P}$ goes to zero as $H_{\rm P}$ goes to infinity, although $l_{\rm ov}$ itself stays finite.

We would like to emphasize that our ∇ prescription conveniently covers observed stars in the whole mass range of 1.5 to 7 ${\rm M}_\odot$ with the same value of $\delta_{\rm ov}$: for the evolved components of ζ Aurigae binaries (see Paper II) and of other double-lined eclipsing binaries (see Paper III), as well as for cluster isochrones (see Section 6 of this paper), we find that our models with overshooting provide the best match with a $\delta_{\rm ov}$ value of about 0.12. Typical δ values then range from 0.05 to 0.04, respectively. Also, the ∇ prescription does not distinguish between core or envelope boundaries so that overshooting also extends from convective envelopes (see Fig. 1).

An important test for the reliability of a code is provided by the solar luminosity and radius. However, both of these quantities are also affected by free parameters. The luminosity L of a stellar model depends on the incorporated nuclear reaction rates and the equation of state, but also on the helium abundance in the core, and can thus be adjusted by the choice of the initial helium abundance Y. The radius R (and the effective temperature $T_{\rm eff}$) are affected by the choice of mixing-length parameter α. A solar model computed by our code matches the Sun with an initial helium abundance of $Y = 0.2812$ ($X = 0.70$, $Z = 0.0188$, corresponding to the meteoric abundance ratios found by Anders & Grevesse 1989; see Paper I), and $\alpha = 2.0$ at an age of 4.5×10^9 yr. By comparison, more detailed solar models, which in particular meet observed helioseismological properties, require a lower He abundance in the outer layers of the Sun than most stellar evolutionary codes (including our code)

would suggest. One such model includes He-diffusion by gravitational settling and starts with an initial helium abundance Y of only 0.25 (Kosovichev 1993). In fact, the helium abundance in the core region of that model is about the same as in our solar model. The inclusion of He-diffusion can thus account for a discrepancy in Y of about 0.04 (Christensen-Dalsgaard et al. 1993). We may therefore conclude that the luminosity scale of our models is reasonably correct, i.e. we do not need any artificial adjustments of Y.

3 STELLAR MODELS

To avoid confusion, hereafter the term *model* refers to a particular stellar model of mass M and metallicity Z at a certain age t or point in its evolution, e.g. the BFGB (base of the first giant branch) model for $M = 2\,\mathrm{M}_\odot$ and $Z = 0.02$. When the term *track* is used, it refers to the whole sequence of models for a certain mass and metallicity, e.g. the track for $M = 2\,\mathrm{M}_\odot$ and $Z = 0.02$.

With our evolution code as described above, we have computed a series of evolutionary tracks for stellar models with masses M between 0.5 and 50 $\mathrm{M}_\odot$, and with metallicities $Z = 0.0001$, 0.0003, 0.001, 0.004, 0.01, 0.02 and 0.03. The tracks are spaced by approximately 0.1 in $\log M$, except between 0.8 and 2 $\mathrm{M}_\odot$ where the mass spacing is closer (about 0.05 in $\log M$) to resolve the rapidly changing shape of the main sequence (MS) in this mass range.

The initial hydrogen and helium abundances are assumed to be functions of the metallicity as follows: $X = 0.76 - 3.0Z$ and $Y = 0.24 + 2.0Z$, i.e. helium and metal abundances are related by $\Delta Y/\Delta Z = 2.0$. This parametrization adequately spans the range between an approximately primordial chemistry ($X = 0.76$, $Y = 0.24$, $Z = 0$), and a quasi-solar abundance ($X = 0.70$, $Y = 0.28$, $Z = 0.02$), slightly extrapolated towards higher metallicity.

The ratio of mixing length over pressure scaleheight (α) is assumed to be independent of the specific physical conditions and $\alpha = 2.0$ has been adopted as an appropriate value for all our models. Both the choice of mixing length and of helium abundance as above lead to a very good match of the solar model (using $Z = 0.0188$), as discussed in Section 2. As mentioned before, we do not take into account helium diffusion through gravitational settling effects.

We have also neglected stellar wind mass loss for the computations presented here. From experiments with 1–3 times the Reimers (1976) mass-loss rate, we found that the corresponding effect on the mass, and consequently on the model properties, is very small (less than 0.1 $\mathrm{M}_\odot$) for most of the evolutionary tracks, except for the final and brief asymptotic giant branch (AGB) stages. Since mass-loss rates for such late-type stars are very uncertain, we prefer to model the mass loss of FGB and AGB stars by interpolation between models, because (1) this makes it easy to experiment with different mass-loss rates, and (2) the simple structure of such stars makes this approach completely adequate.

As well as this set of models, which we label the standard (STD) models, we have computed a similar set of models with a moderate amount of enhanced mixing beyond the Schwarzschild boundary of the convective regions. We label this set the overshooting (OVS) models, although we emphasize again that we do not believe that such enhanced mixing is necessarily a result of convective overshooting alone. We found (Paper II) that the best correspondence with the properties of ζ Aurigae binaries (spanning a mass range of 2.5 to 7 $\mathrm{M}_\odot$) occurs for a value of $\delta_{\mathrm{ov}} \approx 0.12$. For consistency, we adopt this amount of enhanced mixing in our entire set of overshooting models. The differences from the standard models become negligible below about 1 $\mathrm{M}_\odot$. As discussed below, however, our standard models may be the better choice for even larger masses, because there is evidence from cluster isochrones that overshooting begins gradually between 1.1 and 1.6 $\mathrm{M}_\odot$.

The starting model for all computed tracks is the zero-age main sequence (ZAMS). The ZAMS models were constructed using the procedure described by Tout et al. (1996). In all but a very few cases the calculations proceeded without interruption either to central carbon-burning for massive stars, to the start of the first thermal pulse on the AGB for intermediate-mass stars, or to the degenerate He flash for low-mass stars. Our implicit algorithm often skips the AGB thermal pulses altogether, in which case (owing to the absence of mass loss) the intermediate-mass models evolve uninterruptedly to the degenerate C flash at the tip of the AGB. This was the case for all tracks with $Z = 0.02$ and 0.03, but generally not for lower metallicities. We made no attempt to compute through a thermal pulse if it occurred.

For the low-mass stars we were unable to compute through the He flash. Instead we constructed zero-age horizontal branch (ZAHB) models by a roundabout way in order to calculate the He-burning and AGB evolution of such stars. We start with the lowest-mass model which ignites helium non-degenerately (about 2.5 $\mathrm{M}_\odot$ for the STD models, about 2 $\mathrm{M}_\odot$ for the OVS models) and evolve it up to the point where He just ignites, without allowing He to be consumed. These models have homogeneous He cores of about 0.33 $\mathrm{M}_\odot$. We then take mass from them, keeping the core mass constant, until the total mass equals the mass of the He-flash model whose evolution we wish to continue. We then give the envelope the same chemical composition as the He-flash model and subsequently let the core mass grow up to the value of the core mass in the He-flash model (close to 0.5 $\mathrm{M}_\odot$). This final model is our ZAHB model. This procedure, and particularly the order of the steps described above, is important to ensure a ZAHB model with a chemical profile that matches as closely as possible that of the pre He-flash model with, in particular, the sharp composition gradient at the position of the H-burning shell. However, in no case is an exact match of this profile achieved, and this no doubt introduces a small error in the post He-flash evolution. These ZAHB models were evolved up to the same stages as for intermediate-mass stars, i.e. either the first thermal pulse (low Z tracks) or the degenerate C flash or envelope exhaustion if pulses were avoided ($Z = 0.02$ and 0.03).

A subset of the resulting OVS tracks in the HRD are shown in Fig. 2 for $Z = 0.02$ and Fig. 3 for $Z = 0.001$. In Paper I we gave a similar figure for the STD tracks with $Z = 0.02$. The complete set of tracks is available in electronic form, and we refrain from publishing tables in this paper. In Section 5 we will describe the form in which the tracks are available, in accordance with the need to be able to interpolate correctly between tracks and construct reliable isochrones from them. In the following section we discuss some general results of the calculations as a function of mass and metallicity, and how they depend on our overshooting prescription.

4 RESULTS OF THE ∇ PRESCRIPTION

The effect of enhanced mixing on the evolution of low-mass stars ($M \lesssim 1.7\,\mathrm{M}_\odot$) distinctly differs from that on more massive stars. The low-mass stars have small or negligible convective cores to start with and the difference between our ∇ prescription and other prescriptions for overshooting becomes most apparent here. The greatest influence of overshooting at these masses is on the shape of the MS, in particular the appearance of the 'hook' at central H

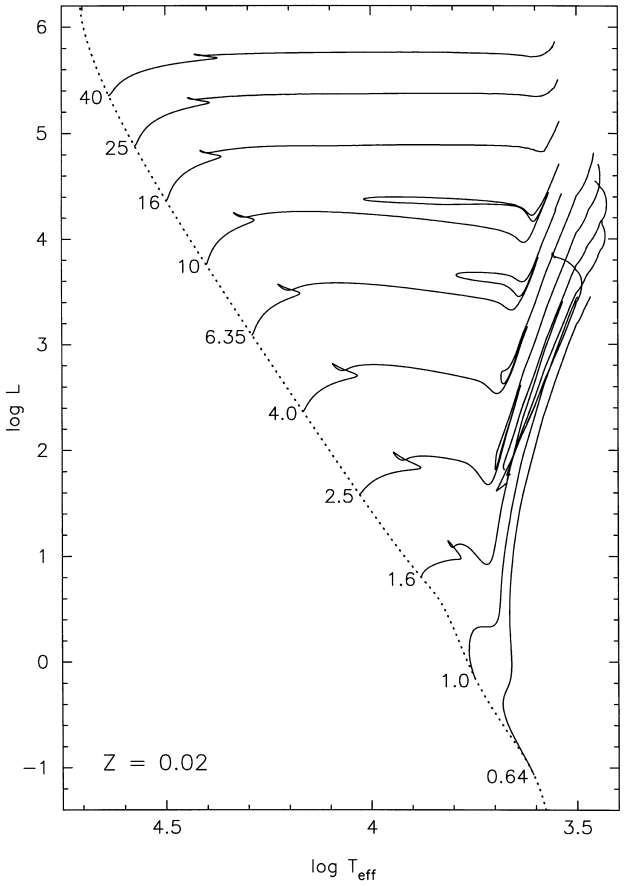

Figure 2. ZAMS (dotted line) and selected OVS evolution tracks (solid lines) for $Z = 0.02$, for masses 0.64, 1.0, 1.6, 2.5, 4.0, 6.35, 10, 16, 25 and 40 $M_\odot$.

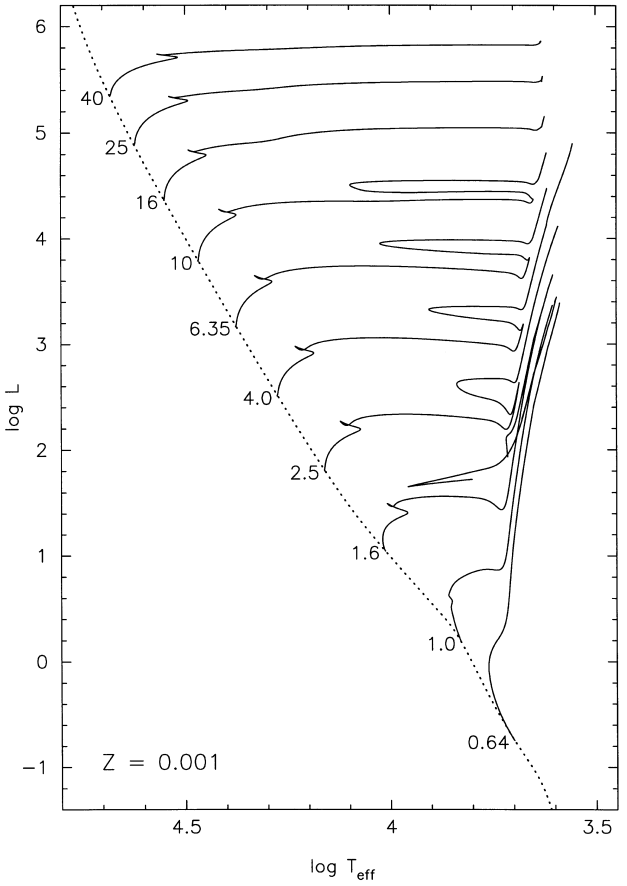

Figure 3. Same as Fig. 2 for $Z = 0.001$. The 1.0 $M_\odot$ post-He flash track has been omitted for clarity.

exhaustion. This feature is a result of the rapid contraction and brightening of a star when H burns out in a convectively mixed core, as H burning quickly moves from the centre to a shell at the edge of the core. In the absence of central convection, or when convective mixing ceases before H exhaustion, the transition from central to shell burning is smooth and there is no MS hook. In Table 1 we list the minimum mass for which the hook appears ($M_{\rm hook}$) as a function of Z for both the STD and OVS models. (These values have been estimated from tracks spaced by approximately 10 per cent in mass, so that the accuracy is probably no better than 3 per cent.)

Models at low and high metallicity also behave somewhat differently. As was discussed in Section 2 (see Fig. 1), the ∇ prescription can induce a small central region that is mixed even in the absence of a convective core because the centre is very close to convective instability. For low metallicity models ($Z \lesssim 0.001$), a tiny convectively unstable core of $\lesssim$0.01 $M_\odot$ is present even for very low stellar masses, 0.4 to 1 $M_\odot$. However, in both cases, the extended mixing region leads to a slower decrease of the central H abundance than in an STD model. In the low-Z STD models the initial convective core shrinks and, for $M < M_{\rm hook}$, disappears before central H-exhaustion thus avoiding the MS hook. The effect of the extended mixing region is to prolong the lifetime of the convective core, so that it may survive until central H exhaustion at lower masses. Therefore, $M_{\rm hook}$ is substantially lower for the OVS models. At high Z, no convective core is initially present for $M \lesssim 1.15\,M_\odot$, but for masses above this limit the core in the STD models tends to *grow* rather than shrink, producing a well-pronounced hook as central H burns out. The extended mixing region can in this case produce a growing convective core in a model of somewhat lower mass after some H has been burnt, even when it was initially absent, so that $M_{\rm hook}$ is slightly lowered for the OVS models as well.

Apart from the hook behaviour, the differences between STD and OVS models at low masses are very small. For $M < M_{\rm hook}$(OVS), the positions in the HRD at any time are virtually indistinguishable and so, therefore, are the lifetimes. The stellar structure is very similar even though the central H abundance initially decreases more slowly in the OVS models. Even for $M < M_{\rm hook}$(STD), the

Table 1. Critical stellar masses (in $M_\odot$) estimated from our calculations. $M_{\rm hook}$ is given for both sets of models, the last four columns are for the OVS models only. See text for an explanation of the symbols.

Z	STD $M_{\rm hook}$	OVS $M_{\rm hook}$	$M_{\rm HeF}$	$M_{\rm FGB}$	$M_{\rm up}$	$M_{\rm ec}$
0.0001	1.65	1.10	1.89	4.8	5.0	6.8
0.0003	1.45	1.05	1.83	8.1	5.0	6.8
0.001	1.30	0.95	1.80	10.3	5.0	6.8
0.004	1.20	0.95	1.87	11.6	5.4	7.0
0.01	1.15	0.98	1.96	12.5	5.8	7.6
0.02	1.15	1.02	1.99	(13)	6.1	7.9
0.03	1.15	1.05	2.03	(13)	6.3	8.1

Table 2. Critical turning points and equivalent model numbers along evolution tracks.

model	no.	description
A	1	ZAMS.
B	21	Red point of the MS hook for $M > M_{\rm hook}$, i.e. the model with minimum $T_{\rm eff}$. For $M < M_{\rm hook}$, B = C.
C	25	TAMS (terminal-age main sequence), or blue point of the MS hook for $M > M_{\rm hook}$, i.e. maximum $T_{\rm eff}$. For $M < M_{\rm hook}$, the model with $X_c = 0.001$.
E	40	BFGB for $M < M_{\rm FGB}$. For $M \geq 1.6\,{\rm M}_\odot$, a local minimum in L. For $M < 1.6\,{\rm M}_\odot$ there is often no clear minimum, so we take the model where the mass of the convective envelope becomes greater than one third of the entire envelope mass (defined as the mass above which $X > 0.1$). For $M > {\rm M}_{\rm FGB}$, E = L and all intermediate points are equivalent.
F	54	Temporary reversal or slowing-down ('hiccup') of the FGB ascent in low-mass stars, when the H-burning shell catches up with the composition jump left by the retreating convective envelope. For $M > M_{\rm HeF}$, F = H = J.
G	55	End of FGB 'hiccup'. Sometimes F and G correspond to a local maximum and minimum in L.
H	70	TFGB (tip of the FGB), corresponding to He ignition for $M < M_{\rm FGB}$, i.e. the He flash for $M < M_{\rm HeF}$.
J	71	Start of CHeB; this is the ZAHB for $M < M_{\rm HeF}$.
L	81	Start of blue phase of CHeB, if there is one. For $M < M_{\rm FGB}$: start of the blue loop, defined as the model with a maximum in $\vert L_{\rm th}\vert$, sometimes a local maximum in R. For $M > M_{\rm FGB}$: equivalent to He-ignition, defined as the model with maximum R if this occurs, or else the start of slow evolution across the HG, identified by eye.
M	93	Blue point of CHeB loop, i.e. maximum $T_{\rm eff}$. For $M > M_{\rm FGB}$, sometimes M = L.
N	105	End of blue phase of CHeB, as the giant branch is reached. Defined as a maximum in $\vert L_{\rm th}\vert$, or a minimum in L.
P	117	BAGB (base of the AGB) or end of CHeB, defined as a local minimum in the He-burning luminosity $L_{\rm He}$, or – if this occurs before the BAGB, for very low Z – the model where the giant branch is reached, in which case P = N.
R	119	Local maximum in L, just before the H-burning shell extinguishes.
S	121	Local minimum in L shortly after R, when shell He-burning has stabilized.
T	133	Start of second dredge-up on the AGB, the model where the convective envelope reaches the extinguished H-shell. In the absence of a second dredge-up ($M \gtrsim 3{\rm M}_\odot$), T = U = V.
U	138	End of second dredge-up, in some cases corresponding to a maximum in L as the H shell is reignited.
V	141	Start of double-shell burning, i.e. start of the thermally-pulsating AGB (TPAGB). Since thermal pulses do not usually occur with our code, V is defined as the model where the rate of growth of the He core reaches 90 per cent of the rate of growth of the C–O core. This corresponds approximately to $L_{\rm H} = 5L_{\rm He}$.
W	151	Carbon ignition, degenerate for $M < M_{\rm up}$ in which case it is the final model in the absence of mass loss. For $M > M_{\rm up}$, defined as the model where the C-burning luminosity equals the total luminosity ($L_{\rm C} = L$) or the model where the C abundance in the centre or burning shell drops by 0.02, whichever occurs first.
Z	155	Final model for $M > M_{\rm up}$.

evolution *after* the OVS hook and the lifetime up to and on the FGB, is again essentially the same for both types of model. This is probably caused by the fact that the H-exhausted core is in either case smaller than the Schönberg–Chandrasekhar limit, so that post-MS models are in thermal equilibrium and the structure is very similar for the same He core mass. The only other noticeable differences in the OVS models are that (1) the 'hiccup' in the FGB ascent, when the H-burning shell catches up with the composition jump left by the retreating convective envelope, occurs at somewhat lower luminosity owing to extended mixing from the envelope, and (2) the lifetime of the CHeB (central helium burning) phase, or horizontal branch, is extended by 10 to 20 per cent owing to overshooting from the He-burning core.

Only when the mass substantially exceeds $M_{\rm hook}$(STD), and the convective core is large, does the post-MS evolution start to differ in the way discussed in Paper II: the larger fuel reservoir available with overshooting extends the MS lifetime, and results in a larger He core mass and thus faster evolution and higher luminosities in later evolutionary phases. Another manifestation of enhanced mixing is that some critical masses are substantially lowered with respect to standard models. These are, e.g., the maximum mass of a star experiencing a degenerate He flash at the tip of the FGB ($M_{\rm HeF}$), the maximum mass for which He ignition occurs on the FGB ($M_{\rm FGB}$), the minimum mass undergoing non-degenerate C ignition ($M_{\rm up}$), and the minimum mass of such a star avoiding electron capture on Ne and Mg in the core ($M_{\rm ec}$) and continuing nuclear burning until an Fe core is formed. In Table 1 we give the estimated values of these critical masses for our OVS models as a function of Z.

We define $M_{\rm HeF}$ as the mass for which the luminosity at the FGB tip reaches a minimum and the core mass at He ignition is about $0.33\,{\rm M}_\odot$, so that stars of slightly lower mass ignite He under semi-degenerate conditions at core masses between 0.33 and $0.45\,{\rm M}_\odot$. The values of $M_{\rm HeF}$ in Table 1 are estimated with the aid of a few additional tracks calculated at $0.1\,{\rm M}_\odot$intervals, and are accurate up to about $0.03\,{\rm M}_\odot$. The other critical masses have an estimated accuracy of 0.2–$0.3\,{\rm M}_\odot$.

Stars with $M > M_{\rm FGB}$ ignite He in the Hertzsprung gap (HG), avoiding a FGB phase. For $Z \lesssim 0.001$ there is a smooth transition between the post-FGB blue loop at $M < M_{\rm FGB}$ and the blue CHeB phase for larger masses. For $Z \gtrsim 0.004$, however, there is a discontinuity in mass because the blue loop disappears rather abruptly at $\sim 11\,{\rm M}_\odot$, and for masses between $\sim 11\,{\rm M}_\odot$ and $M_{\rm FGB}$ there is no blue phase of CHeB. For $Z \gtrsim 0.02$ and $M \gtrsim 11\,{\rm M}_\odot$ the blue phase of CHeB does not last long and $M_{\rm FGB}$ has little meaning because He burning takes place almost entirely on the red (super)-giant branch.

$M_{\rm up}$ and $M_{\rm ec}$ refer to the expected final stages of evolution, and their values have been estimated from the size of the He core mass after central He exhaustion. It appears that, quite independently of Z, a He core mass in excess of about $1.6\,{\rm M}_\odot$ has a C–O core that ignites C off-centre when it has a mass of $\gtrsim 1.08\,{\rm M}_\odot$. This critical C–O core mass is very similar to that found in previous studies (e.g. Becker & Iben 1980). A more detailed study of the evolution of He stars with the same overshooting prescription will be published separately (Pols, in preparation), and we refer to that paper for details. Although our calculations do not extend this far, it is

expected that stars with $M_{\rm up} < M < M_{\rm ec}$ produce degenerate cores consisting mainly of O, Ne and Mg (and perhaps some C if C-burning fails to reach the centre). Such stars continue their evolution on the AGB after C-burning (Nomoto 1984), and may produce a neutron star in a supernova explosion by electron capture on Mg^{24} if the core mass reaches the Chandrasekhar mass. That depends, however, on how much mass the stars in this mass range lose on the upper AGB – they may also produce a white dwarf.

The value of $M_{\rm ec}$ has been estimated from the condition that the He core mass is about 2.2 $M_\odot$, above which C ignites in the centre and C-burning produces an O-Ne core larger than the Chandrasekhar mass (Pols, in preparation). These stars are expected to ignite Ne non-degenerately, followed by successive nuclear burning phases and the eventual formation of an Fe core. This core will collapse owing to photodisintegration, producing a neutron star in a supernova explosion.

5 INTERPOLATION AND ISOCHRONE CONSTRUCTION

Isochrones can be constructed by interpolation in mass between stellar tracks. In order to get reliable isochrones, the selection of models from the computed tracks requires careful consideration. To obtain the point on an isochrone corresponding to, say, the BFGB, we have to make sure we interpolate between the BFGB models of the tracks bracketing the mass for which $t = t_{\rm BFGB}$. We define a number of critical models or turning points on each evolution track and assign the same equivalent model number to each critical point for all masses and metallicities. When we construct an isochrone we always interpolate in mass and metallicity between equivalent models. Without such careful selection of models, interpolation may obliterate some of the structure present in the tracks and lead to incorrect results, *even* if the models along each track are very densely spaced.

The turning points and equivalent model numbers along each track are defined and selected according to the criteria summarized in Table 2. In between each of these turning points we select a corresponding number of models in such a way that both the shape of the track and the speed of evolution across the track between turning points can be well represented by linear interpolation with a minimum number of points. In practice this is achieved by selecting models which are close to equal intervals of a well-chosen spacing function. We use a spacing function of the form

$$f = \sum_i \frac{t_i - t_{i-1}}{\Delta t} + a\left(\left|\log\frac{L_i}{L_{i-1}}\right| + 4\left|\log\frac{T_{{\rm eff}\,i}}{T_{{\rm eff}\,i-1}}\right|\right), \qquad (1)$$

where the sum extends over all models between two adjacent turning points, and Δt is the total time interval between these turning points. By adjusting the parameter a we can achieve a balance between selecting models that are not too far apart either in L and $T_{\rm eff}$ or in time. In cases where two or more turning points are equal (e.g. models E through L for massive stars), obviously no models are selected between them. By assuming, however, that they exist and are all equal, an accurate interpolation is possible between such a track and an adjacent one for which the turning points are different.

In order to obtain a track with arbitrary mass and metallicity intermediate to the grid values, it is then sufficiently accurate to interpolate $\log L$, $\log T_{\rm eff}$, $\log t$ etc., bi-linearly in $\log M$ and $\log Z$ between equivalent models on the bracketing tracks. In order to construct an isochrone for a certain age t and metallicity Z, we first obtain the tracks for this Z by interpolating the grid in $\log Z$. Subsequently, for each model number j, we determine the mass M_j for which the evolutionary age of that model equals t by interpolating $\log M$ linearly in $\log t$ between models j of the bracketing tracks. Linear interpolation of $\log L$ and $\log T_{\rm eff}$ then gives the basic shape of the isochrone, with a resolution that is generally good enough for the post-MS phases. In order to get better resolution along the MS, we subdivide each mass interval $[M_{j-1}, M_j]$ in equal $\log M$ intervals, such that $\Delta \log M < 0.01$. For each mass point M we then interpolate bi-linearly, in t between models $j-1$ and j and in $\log M$ between the tracks bracketing M.

Since the ZAMS contains more structure than is resolved by the mass spacing of the grid tracks, especially between 1 and 2 $M_\odot$, we have to correct the MS models for the detailed ZAMS shape. For each grid metallicity we have computed ZAMS models much more closely spaced in mass, by about 0.005 in $\log M$, as described by Tout et al. (1996). For each isochrone point with equivalent model number $n \leq 21$ (i.e. before model B) we determine the ZAMS luminosity L_Z and radius R_Z by interpolating linearly in $\log Z$ and $\log M$. We then transform the luminosity L_i for each of these points according to

$$\log L_i' = \log L_{\rm B} + \log(L_i/L_{\rm B})\frac{\log(L_Z/L_{\rm B})}{\log(L_{\rm A}/L_{\rm B})}, \qquad (2)$$

and the radius R_i by a similar formula.

6 OPEN CLUSTERS

In order to test the performance of the isochrones constructed from our models, we have made a comparison with the colour–magnitude diagrams (CMDs) of several well-studied open clusters. We selected intermediate-age and old open clusters with turn-off masses in the range 1.1 to 2.5 $M_\odot$ for two reasons. First, our earlier critical comparisons with eclipsing binaries (Papers II and III) have been restricted mostly to stars more massive than 2 $M_\odot$, or to relatively unevolved stars of lower mass. In particular, we could not distinguish between standard and overshooting models below 2 $M_\odot$. Secondly, relatively old clusters often show a clearly defined and well-populated MS turn-off, giant branch and CHeB clump. In contrast, young clusters usually contain too few stars in the upper HRD to provide a very sensitive test of evolution. Therefore the earlier two tests and the present comparison with cluster CMDs complement each other.

We have taken photometric (V, $B-V$) data for six open clusters from the Open Cluster Database (OCD: Mermilliod 1988), kindly provided and frequently updated by Dr. J.-C. Mermilliod. The data we used usually come from recent CCD photometric studies; we have also used the data for membership and spectroscopic binaries provided in the OCD to eliminate non-members and identify unresolved binaries, as far as possible. In some cases, we have referred to the original studies for additional information.

An important intermediate step in the comparison, and a source of uncertainty, is the conversion from theoretical surface properties (L, $T_{\rm eff}$, $\log g$) to observable magnitudes and colours (M_V, $B-V$). We base our conversion on the extensive set of synthetic stellar spectra computed by Kurucz (1992) on a fine grid of $T_{\rm eff}$, $\log g$ and metallicities. However, the conversion from theoretical spectra to broad-band colours is riddled with difficulties (see e.g. Bell, Paltoglou & Tripicco 1994) and therefore not very accurate. Inaccuracies of the Kurucz $B-V$ colours have been noted before (Worthey 1994). Lejeune, Cuisinier & Buser (1997) have constructed an empirical correction of the grid of colours and bolometric corrections computed from the Kurucz spectra and,

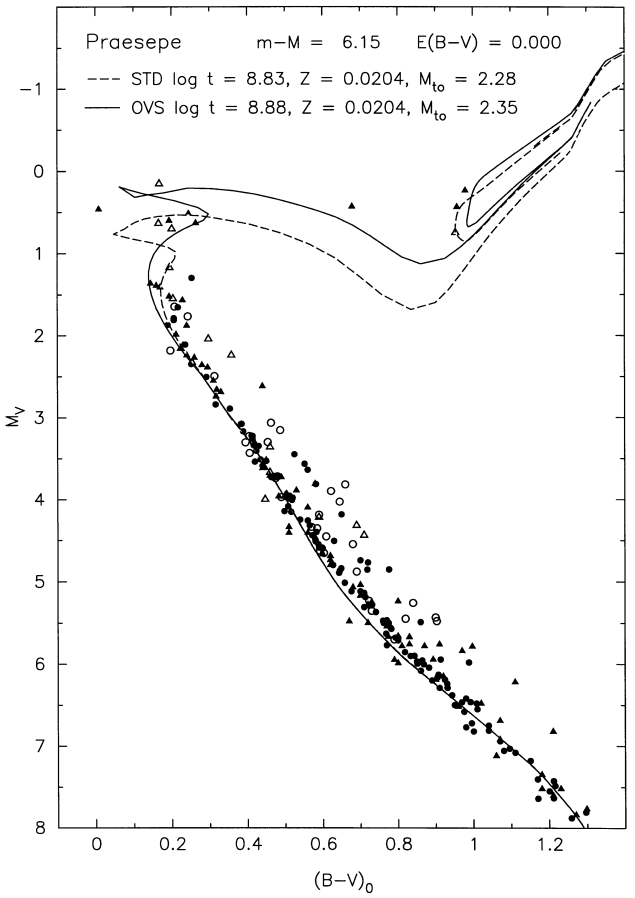

Figure 4. CMD for Praesepe (NGC 2632). Circles show probable members according to proper motion studies and triangles show stars of unknown membership. Filled symbols are apparently single stars and open symbols are spectroscopic binaries. These observational data have been shifted by the indicated values of distance modulus and reddening. Plotted over the data are the best-fitting isochrones for STD models (broken line) and OVS models (solid line). The corresponding turn-off masses are also indicated.

rather than apply the Kurucz tables directly, we use their calibrated tables in our comparison. However, uncertainties of up to 0.05 in $B-V$ may persist (Lejeune et al. 1997) and we note, for instance, that the colour conversion leads to a kink in the giant branch at $B-V \approx 1.3$ that is not present in the original tracks (see e.g. Fig. 4). In the interpretation that follows it is important to keep in mind the uncertainties.

The comparison described in this section is necessarily rather limited, because a more complete study (such as was done recently, e.g., for NGC 3680 by Nordström, Andersen & Andersen 1997) falls outside the scope of this paper. Thus, we pay attention only to the presumed single stars and ignore all effects of duplicity, mass loss and dynamical evolution, such as blue stragglers. We do, however, attempt to be as critical as possible by limiting the number of free parameters to two (distance modulus and age) and using observationally determined values of interstellar reddening $E(B-V)$ and metallicity [Fe/H]. Furthermore, we construct the isochrones in a completely self-consistent manner by transforming the measured [Fe/H] values to Z on the assumption that $Z_\odot = 0.0188$ and $X = 0.76 - 3Z$, which leads to $Z = 0.76/(3.0 + 37.425 \times 10^{-[\mathrm{Fe/H}]})$. We then use the interpolated theoretical isochrone (Section 5) in combination with the synthetic colours interpolated for the same metallicity value. Hence we do not need an artificial shift of solar-metallicity isochrones to account for metallicity effects, as is often necessary in other schemes.

Apart from looking at how well the isochrones fit the shape of the single-star sequence in the CMD, we pay special attention to the relative population along the upper isochrone (the MS turn-off and beyond). This is an important diagnostic for the evolutionary timescale beyond the MS, very sensitive to the amount of enhanced mixing, which would be neglected if we just considered the shape of the isochrone.

6.1 Praesepe

This well-known and well-studied cluster is the youngest in our sample. The metallicity is very nearly solar, [Fe/H] $= 0.038 \pm 0.039$ (Friel & Boesgaard 1992) and the interstellar reddening is negligible. The shape of the MS isochrone, for both STD and OVS models, below the turn-off is quite well-fitted for a distance modulus $m–M = 6.15$, see Fig. 4, down to $M_V = 8.2$ ($\sim 0.65 M_\odot$), below which it becomes too blue (probably owing to pre-MS evolution). The isochrone is slightly too blue in the range $M_V \sim 4.5$ to 6, i.e. around $1\,M_\odot$, by up to 0.04 in $B-V$. This appears to be the case for some of the other clusters as well. Because our models are well-tested against the present Sun, we may possibly ascribe this to uncertainties in the colour conversion (see above).

The STD and OVS isochrones deviate substantially in the turn-off region – yielding turn-off masses of 2.28 and $2.35\,M_\odot$, respectively – but the CMD is sparse enough that both STD and OVS models can be said to fit the shape reasonably well. The implied luminosity of the He-burning giants is also not too different and is consistent with both models. However, the models lead to different interpretations of the brightest six blue stars which appear to be separated by a gap from the rest of the main sequence. The STD isochrone would imply that they have evolved beyond the MS hook, into the shell-H burning phase, although some of them are spectroscopic binaries. In the OVS interpretation, however, they constitute the brightest MS stars before the hook. A consideration of the implied numbers along the isochrone shows that the first interpretation is very unlikely. Invoking the requirement that the mass function be smooth, the STD models imply there should be about five times as many He-burning giants in the clump than stars in the post-hook phase, whereas the numbers are at best equal: at least four post-hook stars and at most four clump stars. This is insensitive to the assumed slope of the mass function. Although the numbers are small, the probability based on Poisson statistics can be shown to be less than 1 per cent. On the other hand, the ratio of upper MS stars to giants is in perfect agreement with the STD models.

6.2 NGC 752

An extensive study of NGC 752 was made by Daniel et al. (1994), who obtained BV photometry and radial velocities and identified numerous spectroscopic binaries and binary candidates. The cluster contains a high proportion of binaries. If these are removed from the CMD the resulting shape of the turn-off clearly shows that the upper MS bends over to the red. This makes NGC 752 an interesting test object for evolution models. We adopt the reddening and metallicity from Daniel et al. (1994), $E(B-V) = 0.035$ and [Fe/H] $= -0.15$, the latter being in close agreement with the spectroscopic determination [Fe/H] $= -0.16 \pm 0.05$ by Friel & Janes (1993). Taking $m - M = 8.3$, the OVS isochrone for an age of 1.58 Gyr fits the shape of the turn-off and the extent of the MS very well when the

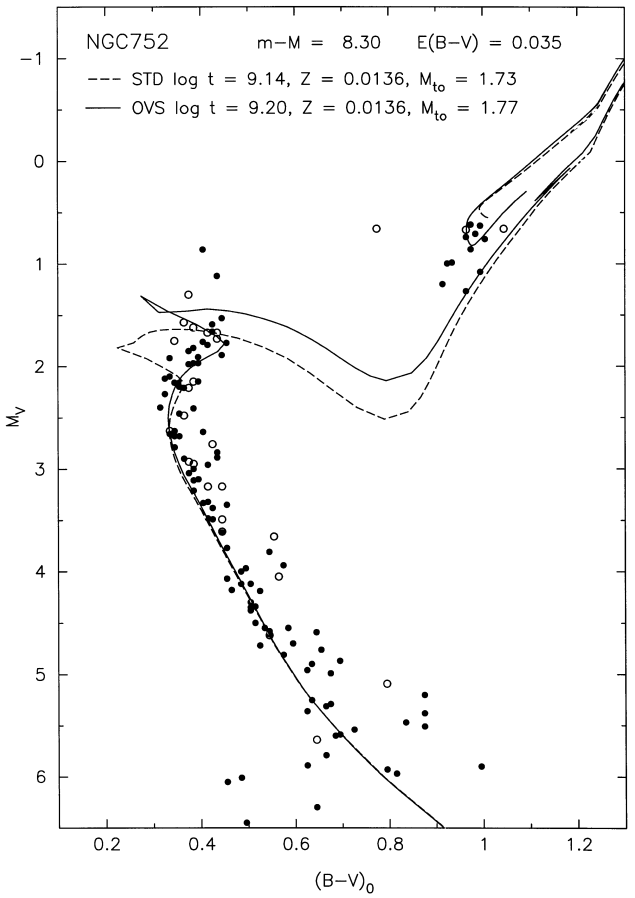

Figure 5. Same as Fig. 4 for NGC 752.

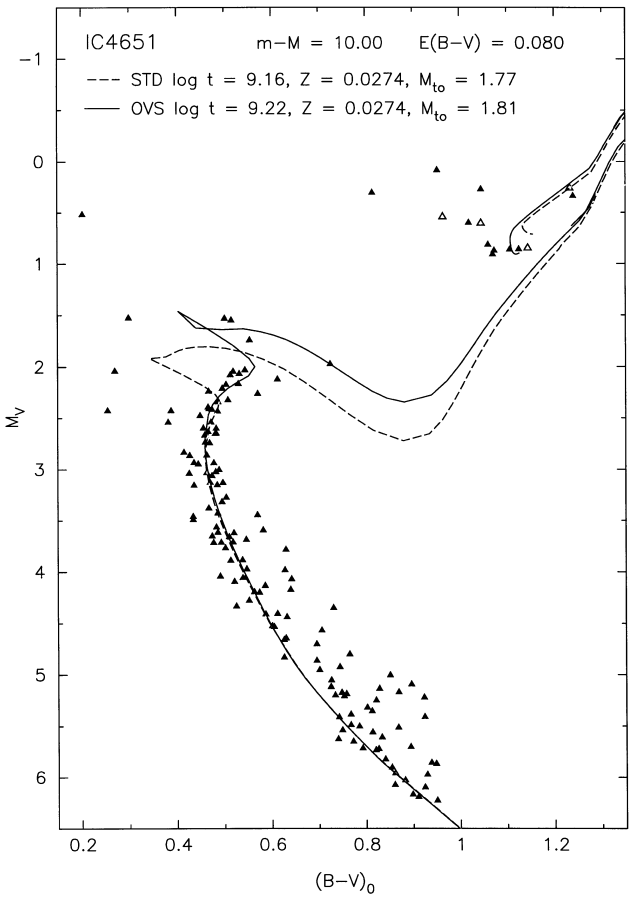

Figure 6. Same as Fig. 4 for IC 4651.

numerous binaries are ignored (see Fig. 5). The position of the red giant clump of CHeB stars is also well matched, apart from three stars slightly fainter and bluer than the clump. The turn-off mass for this isochrone is 1.77 $M_\odot$and the CHeB stars have masses between 1.8 and 1.9 $M_\odot$. This is very close to the maximum He-flash mass for the OVS models and the He-burning luminosity is somewhat lower than for less massive CHeB stars. The STD models, on the other hand, fail to match the shape and extent of the upper MS for any age. Furthermore, the CHeB giants are expected to have significantly higher luminosities. This may be taken as an indication that $M_{\rm HeF}$ is indeed close to 1.9 $M_\odot$, as predicted by the OVS models.

6.3 IC 4651

Although less well-studied for binaries and membership than NGC 752, the CMD of IC 4651 – based on photographic data of Anthony-Twarog et al. (1988), reproduced in Fig. 6 – also shows a very clearly defined upper MS with a characteristic bend. No spectroscopic metallicity determination is available, but from *uvby* photometry Anthony-Twarog & Twarog (1987) found [Fe/H] $= 0.23 \pm 0.02$ and $E(B-V) = 0.088 \pm 0.008$. With these values our isochrones are slightly too red to fit the MS and we have to assume either a lower metallicity or a lower reddening. We therefore adopt [Fe/H] $= 0.18$ (Nissen 1988) and $E(B-V) = 0.08$ and the best-fitting isochrones for these values are shown in Fig. 6. The OVS models at an age of 1.66 Gyr provide a good fit to the shape and extent of the upper MS, whereas the STD models fail to match the shape of the turn-off region at any age. The turn-off mass for this isochrone is 1.80 $M_\odot$. It may be argued that the MS bends over a little less than our OVS isochrone, but this small discrepancy largely disappears if we assume a higher metallicity, [Fe/H] $= 0.23$ and $E(B-V) = 0.06$. The luminosity of the red giant clump is also matched very well, but the isochrone is too red to fit its colour. However, if we adopt the uncorrected Kurucz colours the reddest stars are quite well fitted by the FGB and CHeB clump. There are six giants with quite blue colours, at least two of which are spectroscopic binaries.

6.4 NGC 2420

NGC 2420 is a rich cluster with rather low metallicity, for which deep and accurate CCD photometry was obtained by Anthony-Twarog et al. (1990). Though the CMD (reproduced in Fig. 7) must contain many non-members below $M_V \approx 2$, the MS is very well-defined and clearly bends over at the top. The spectroscopically determined metallicity is [Fe/H] $= -0.42 \pm 0.07$ (Friel & Janes 1993) but the reddening appears to be uncertain: we adopt $E(B-V) = 0.05$ and $m - M = 11.95$ following Anthony-Twarog et al. (1990). The OVS isochrone with an age of 2.35 Gyr fits the shape of the upper MS very well, it also matches the apparent subgiant branch including the gap with the turn-off and the FGB (see also Demarque, Sarajedini & Guo 1994). The largest discrepancy occurs for the CHeB clump, which is fainter by about 0.2 mag than where our isochrones put it (see also Section 6.5 for M 67). The turn-off mass is 1.47 $M_\odot$, the lowest mass for which we find the

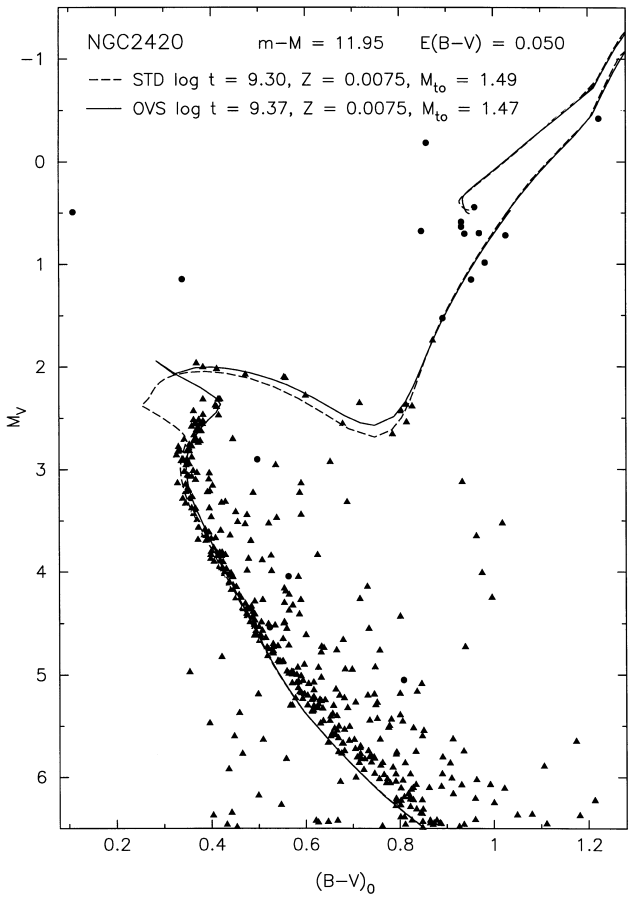

Figure 7. Same as Fig. 4 for NGC 2420.

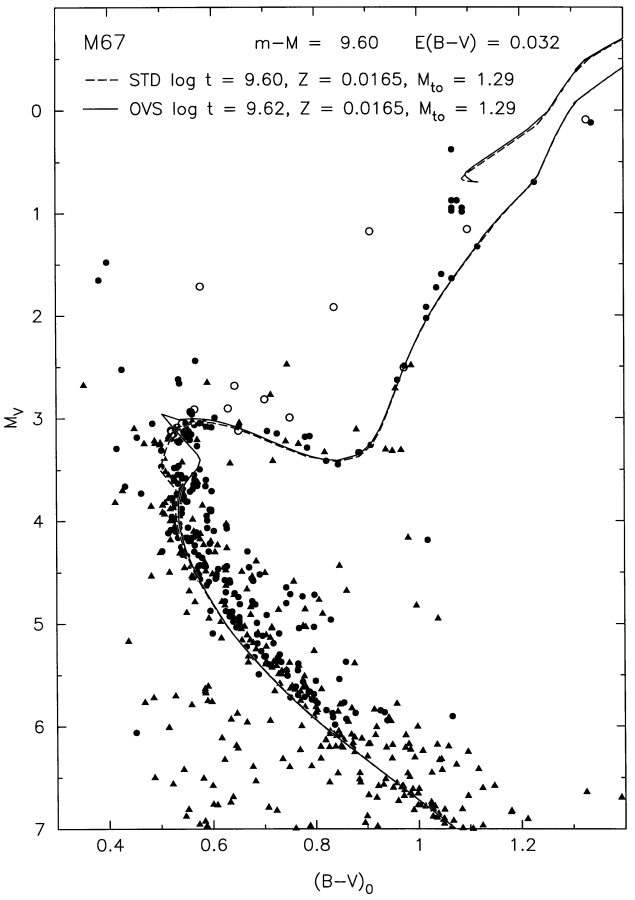

Figure 8. Same as Fig. 4 for M 67.

OVS isochrones to give a better fit than the STD isochrones. At the rather low metallicity of NGC 2420, however, stars of this mass have larger convective cores than at solar metallicity, where a comparative core would require a stellar mass of about 1.6 $M_\odot$.

The subgiant branch (SGB) appears to be a real feature, though it may contain a few binaries (just above the turn-off) and field stars. We stress that, according to the STD isochrone, the SGB should extend to much bluer colours than is observed, and that this blue part (with $B - V < 0.35$) should be the most populated. To quantify this statement, we divide the part of the CMD beyond the MS hook into three regions: A, the blue part of the SGB ($B - V < 0.35$); B, the red part of the SGB including the lower FGB ($B - V > 0.35$ and $M_V > 2.0$), and C, the upper FGB and CHeB clump ($M_V < 2.0$). No stars are observed in region A, while regions B and C contain 14 and 13 stars respectively. With a smooth mass function (assuming a Salpeter slope, but the result is insensitive to this), the STD isochrone predicts about equal numbers of stars in each of these regions (A : B : C = 1.15 : 0.90 : 1.00), i.e. one would expect at least 15 stars in the empty region A. The OVS isochrone correctly predicts no stars in region A (A : B : C = 0.03 : 0.35 : 1.00), but on the other hand underestimates the population of region B by a factor of 2.5 – 3. Although the numbers are small it would appear that, even though the OVS correctly models the shape and extent of the upper MS and SGB, it predicts a speed of evolution across the HG that is too fast.

6.5 M 67

M 67 is significantly older than NGC 2420 and shows a clear gap in the upper MS which must be identified with the MS hook, the stars above it being in a shell H-burning phase. For old clusters like this and NGC 188, this gap and the SGB form the only prominent feature depending on overshooting, the differences for more advanced evolution being largely wiped out at the base of the FGB. We take the CCD photometric data of Montgomery, Marschall & Janes (1993), extending to very faint magnitudes (Fig. 8). The metallicity is slightly sub-solar: we adopt [Fe/H] $= -0.06$ and $E(B - V) = 0.032$ from Nissen, Twarog & Crawford (1987). This metallicity determination is in between the spectroscopic values by Hobbs & Thorburn (1991) and Friel & Janes (1993). With $m - M = 9.6$ the STD isochrone for an age of 4.0 Gyr gives a good fit to the upper MS just below the turn-off, to the subgiant branch and to the MS below $M_V = 6.0$, although it is slightly too blue between $M_V = 6.0$ and 4.5, as noted for Praesepe above. The same is true for an OVS isochrone which is 5 per cent older. The FGB is also well-fitted, except for the brightest stars where the kink in the colour conversion tables occurs. However, the CHeB clump is about 0.3 mag fainter than expected. Part of this discrepancy might be attributed to mass loss on the upper FGB (which might also be the case for NGC 2420), but to explain the entire discrepancy this way requires unreasonably large mass-loss rates; also note the warning by Carraro et al. (1996). For the moment this discrepancy remains a mystery.

Turning back to the turn-off region, it appears that neither the STD nor the OVS isochrone fits the position of the gap perfectly, the STD models perhaps coming somewhat closer, especially if we also take into account the effect that unresolved binaries have on this

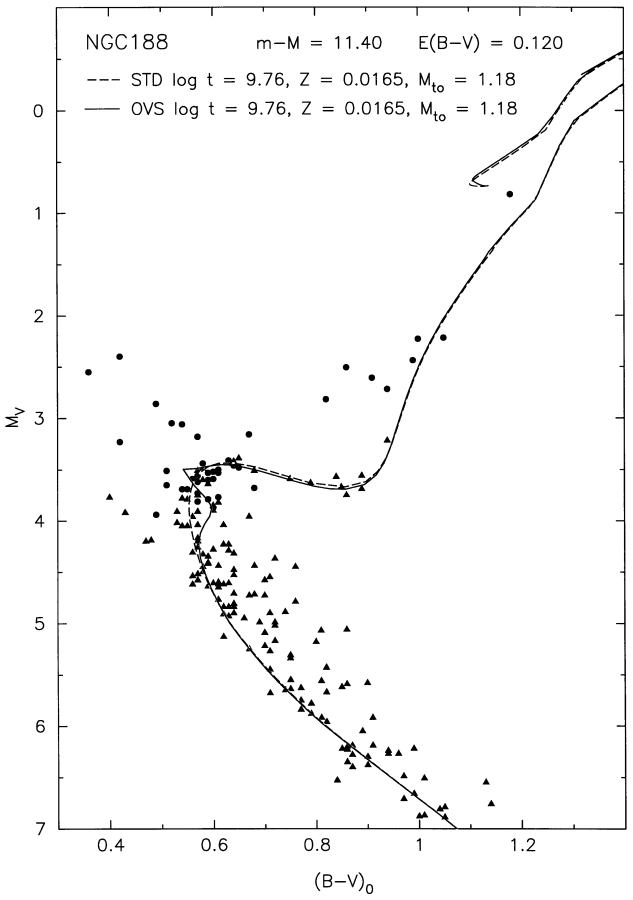

Figure 9. Same as Fig. 4 for NGC 188.

region (Morgan & Eggleton 1978). The turn-off mass for both is $1.29\,M_\odot$, if we interpret this as the mass at the subgiant point with maximum brightness. The MS hook or gap occurs at $1.22\,M_\odot$, and the CHeB clump has a mass of about $1.35\,M_\odot$. The numbers of stars above the gap, compared to the HG and the FGB, are also in better agreement with the STD models. We performed star counts in regions similar to those defined in Section 6.4, but with the boundary between regions A and B at $B-V=0.60$ and between B and C at $M_V=3.0$. Excluding the known binaries and probable non-members, we count 34, 17 and 19 stars in regions A, B and C respectively. The STD and OVS isochrones predict very similar numbers in regions B and C, but very different in region A – the expected ratios are A : B : C = 2.5 : 0.8 : 1.0 and 0.2 : 0.7 : 1.0 for the STD and OVS isochrones respectively. Hence, the population of stars above the gap is slightly overestimated (by a factor of 1.5) for the STD models, but is underestimated by a factor of 10 for the OVS models. We may conclude from this that the amount of core overshooting in the mass range 1.2 to $1.3\,M_\odot$ might not be negligible, but is at least significantly smaller than is given by our prescription with $\delta_{ov}=0.12$.

6.6 NGC 188

No accurate determination of the metallicity exists. The spectroscopic measurement by Hobbs, Thorburn & Rodriguez-Bell (1990) $[Fe/H]=-0.12\pm0.16$ has large errors. We therefore adopt the value of −0.06 from the Lyngå (1985) catalogue and, following Twarog & Anthony-Twarog (1989), $E(B-V)=0.12$. The best-fitting isochrones for both sets of models have the same age of 5.8 Gyr for a distance modulus $m-M=11.4$ (Fig. 9). As for M 67, the morphology of both sets of models is very similar, except at the turn-off region. The OVS isochrone implies a gap in the MS around $M_V=3.7$, in contrast to the STD models for which no gap is expected. Any evidence for a gap would put it at a fainter magnitude, about 4.1. Stars in this region have masses between 1.1 and $1.18\,M_\odot$, and we may conclude that there is no significant evidence for core overshooting at these masses.

7 SUMMARY AND CONCLUSIONS

We have presented an extensive grid of stellar evolution models, based on a different prescription for enhanced mixing and computed with an efficient evolution code. From these models, isochrones for arbitrary age and metallicity (within the bounds of the grid) can be constructed by interpolation, according to the procedure described in Section 5. Several critical tests of the models and isochrones have been performed, as discussed in Papers II and III and in Section 6 of this paper.

Based on these tests, we come to the following conclusion: for masses above $1.5\,M_\odot$, the OVS models provide a good fit to the data for a single value of the free parameter $\delta_{ov}=0.12$ (open clusters Praesepe, NGC 752, IC 4651 and NGC 2420), in excellent agreement with the results of Papers II and III. Between 1.3 and $1.1\,M_\odot$, STD isochrones appear to give the better fits (M 67 and NGC 188), but the differences between the two sets of models become much less significant at these low masses. The mass at which enhanced mixing sets in may depend somewhat on metallicity, as discussed for NGC 2420 (Section 6.4). Further empirical tests are desirable for the mass range 1.1 to $1.6\,M_\odot$, including a variety of metallicities, to clarify the onset of enhanced mixing from convective cores on the main sequence.

All models described in this paper are available in electronic form through CDS (`http://cdsweb.u-strasbg.fr/`), or on request by email to the first author, who will provide (by ftp) a package of tables including a FORTRAN code for isochrone construction.

ACKNOWLEDGMENTS

We would like to thank J. C. Mermilliod for making his Open Cluster Database available and sending us regular updates and extensions. We also thank Th. Lejeune for sending us the empirically corrected colour conversion tables. CAT is very grateful for an advanced fellowship from PPARC. KPS acknowledges support from the DFG under grant no. Se420/12-1.

REFERENCES

Aarseth S. J., 1996, in Hut P., Makino J., eds, Proc. IAU Symp. 174, Dynamical Evolution of Star Clusters. Kluwer, Dordrecht p. 161
Alexander D. R., Ferguson J. W., 1994a, in Jorgensen U. G., ed., Molecules in the Stellar Environment. Springer-Verlag, Berlin p. 149
Alexander D. R., Ferguson J. W., 1994b, ApJ, 437, 879
Anders E., Grevesse N., 1989, Geochim. Cosmochim. Acta, 53, 197
Anthony-Twarog B. J., Twarog B. A., 1987, AJ, 94, 1222
Anthony-Twarog B. J., Mukherjee K., Twarog B. A., Caldwell N., 1988, AJ, 95, 1453
Anthony-Twarog B. J., Kaluzny J., Shara M. M., Twarog B. A., 1990, AJ, 99, 1504
Baker N., Temesvary S., 1966, Tables of Convective Stellar Envelopes. Goddard Inst. for Space Studies NASA, New York

Becker S. A., Iben I., Jr., 1980, ApJ, 237, 111
Bell R. A., Paltoglou G., Tripicco M. J., 1994, MNRAS, 268, 771
Böhm-Vitense E., 1958, Z. Astrophys., 46, 108
Bressan A., Fagotto F., Bertelli G., Chiosi C., 1993, A&AS, 100, 647
Canuto V. M., Mazzitelli I., 1991, ApJ, 370, 295
Canuto V. M., Mazzitelli I., 1992, ApJ, 389, 724
Carraro G., Girardi L., Bressan A., Chiosi C., 1996, A&A, 305, 849
Caughlan G. R., Fowler W. A., 1988, At. Data Nucl. Data Tables, 40, 284
Caughlan G. R., Fowler W. A., Harris M. J., Zimmerman B. A., 1985, At. Data Nucl. Data Tables, 35, 198
Chiosi C., 1992, ARA&A, 30, 235
Christensen-Dalsgaard J., Proffitt C. R., Thompson M. J., 1993, ApJ, 403, L75
Claret A., 1995, A&AS, 109, 441
Daniel S. A., Latham D. W., Mathieu R.D, Twarog B. A., 1994, PASP, 106, 281
Demarque P., Sarajedini A., Guo X. J., 1994, ApJ, 426, 165
Eggleton P. P., 1971, MNRAS, 151, 351
Eggleton P. P., 1972, MNRAS, 156, 361
Eggleton P. P., 1973, MNRAS, 163, 179
Eggleton P. P., 1996, in Hut P., Makino J., eds, Proc. IAU Symp. 174, Dynamical Evolution of Star Clusters. Kluwer, Dordrecht p. 213
Eggleton P. P., Faulkner J., Flannery B. P., 1973, A&A, 23, 325
Eggleton P. P., Fitchett M. J., Tout C. A., 1989, ApJ, 347, 998
Fliegner J., Langer N., 1995, in van der Hucht K. A., Williams P. M., eds, Proc. IAU Symp. 163, Wolf-Rayet Stars. Kluwer, Dordrecht p. 326
Friel E. D., Boesgaard A. M., 1992, ApJ, 387, 170
Friel E. D., Janes K. A., 1993, A&A, 267, 75
Han Z., Podsiadlowski P., Eggleton P. P., 1994, MNRAS, 270, 121
Hobbs L. M., Thorburn J. A., 1991, AJ, 102, 1070
Hobbs L. M., Thorburn J. A., Rodriguez-Bell T., 1990, AJ, 100, 710
Hünsch M., Schröder K.-P., 1996, A&A, 309, L51
Iglesias C. A., Rogers F. J., 1996, ApJ, 464, 943
Itoh N., Adachi T., Nakagawa M., Kohyama Y., Munakata H., 1989, ApJ, 339, 354 (erratum 1990, ApJ, 360, 741)
Itoh N., Mutoh H., Hikita A., Kohyama Y., 1992, ApJ, 395, 622 (erratum 1993, ApJ, 404, 418
Itoh N., Hayashi H., Nishikawa A., Kohyama Y., 1996, ApJS, 102, 411
Kosovichev A. G., 1993, MNRAS, 265, 1053
Kippenhahn R., Weigert A., 1991, Stellar Structure and Evolution, 2nd edn. Springer Verlag, Berlin
Kurucz R. L., 1992, in Barbuy B., Renzini A., eds, Proc. IAU Symp. 149, The Stellar Populations of Galaxies. Kluwer, Dordrecht p. 225
Lejeune T., Cuisinier F., Buser R., 1997, A&AS, 125, 229
Lyngå G., 1985, in van Woerden H., Allen R. J., Burton W. B., eds, Proc. IAU Symp. 106, The Milky Way Galaxy. Reidel, Dordrecht p. 143
Mermilliod J.-C., 1988, Bull. Inf. CDS, 35, 77
Meynet G., Mermilliod J.-C., Maeder A., 1993, A&AS, 98, 477
Montgomery K. A., Marschall L. A., Janes K. A., 1993, AJ, 106, 181
Morgan J. G., Eggleton P. P., 1978, MNRAS, 182, 219
Nissen P. E., 1988, A&A, 199, 146
Nissen P. E., Twarog B. A., Crawford D. L., 1987, AJ, 93, 634
Nomoto K., 1984, in Chiosi C., Renzini A., eds, Stellar Nucleosynthesis. Reidel, Dordrecht, p. 239
Nordström B., Andersen J., Andersen M. I., 1997, A&A, 322, 460
Pols O. R., Tout C. A., Eggleton P. P., Han Z., 1995, MNRAS, 274, 964 (Paper I)
Pols O. R., Tout C. A., Schröder K.-P., Eggleton P. P., Manners J., 1997, MNRAS, 289, 869 (Paper III)
Reimers D., 1976, Mem. Soc. roy. Liège, 6e Ser., 8, 369
Rogers F. J., Iglesias C. A., 1992, ApJS, 79, 507
Schaller G., Schaerer D., Meynet G., Maeder A., 1992, A&AS, 96, 269
Schröder K.-P., Pols O. R., Eggleton P. P., 1997, MNRAS, 285, 696 (Paper II)
Seaton M., Yan Y., Mihalas D., Pradhan A. K., 1994, MNRAS, 266, 805
Shaviv G., Salpeter E. E., 1973, ApJ, 184, 191
Singh H. P., Roxburgh I. W., Kwing L. C., 1994, A&A, 281, L73
Talon S., Zahn J. P., Maeder A., Meynet G., 1997, A&A, 322, 109
Tout C. A., Pols O. R., Eggleton P. P., Han Z., 1996, MNRAS, 281, 257
Tout C. A., Aarseth S. J., Pols O. R., Eggleton P. P., 1997, MNRAS, 291, 732
Twarog B. A., Anthony-Twarog B. J., 1989, AJ, 97, 759
VandenBerg D. A., 1991, in Janes K., ed., in ASP Conf. Ser. 13, The Formation and Evolution of Star Clusters. Astron. Soc. Pac., San Francisco, p. 183
Worthey G., 1994, ApJS, 95, 107

This paper has been typeset from a TEX/LATEX file prepared by the author.